JOURNAL OF NANO AND MATERIALS SCIENCE RESEARCH
Volume 3, No.2 (Special Issue, 2025), pp. 7 – 14
Available online at journals.nanotechunn.com/jnmsr

ORIGINAL ARTICLE

Extraction And Purification of Various Natural Dyes For The Optimization Of Solar Cell Performance

R. A. Akwolu[a,], K. P. Alor[b], C. O. Ayogu[a], P. U. Asogwa[a]*

[a] *Department of Physics and Astronomy, University of Nigeria Nsukka, Nsukka 410001, Nigeria*
[b] *Department of Physics and Industrial Physics, Nnamdi Azikiwe University, Awka 420110, Nigeria*

KEYWORDS

Anatase,
Lawsoniainermis,
Baphianitida,
Indigoferatinctoria,

ARTICLE HISTORY

Received: August 02, 2024
Revised: December 13, 2024
Accepted: June 06, 2025
Published: June 11, 2025

ABSTRACT

Dye-sensitized solar cells (DSSCs) have been the subject of much research and growing attention in recent decades due to their comparably easy fabrication, low toxicity, easy preparation, and relatively low cost. The extraction, purification, and characterization of dyes from various plant sources for use for solar cell applications are investigated in this work. The dyes were applied on a TiO_2 layer using a straightforward drop-casting approach. The anatase crystallite structure with a mesoporous shape was successfully deposited, as demonstrated by structural investigations utilizing XRD on the TiO_2 layer. According to Electrochemical Impedance Spectroscopy (EIS) investigations, pure cells had the longest electron lifetime and the lowest recombination resistance, which is responsible for the continuous electron transfer across the oxide layer over a greater distance and the improvement of the power conversion efficiency (PCE). I-V characterizations were used to estimate the photovoltaic parameters and the efficiencies of the devices, the overall best performance of $\eta \sim 1.74$ % was obtained from the cell fabricated with Lawsoniainermis dye extract.

1 Introduction

Due to the significant toxic waste that silicon and thin-film solar cells produce once they break down, they have the potential to cause environmental issues in the future. Another illustration is the quantity of waste generated in the production of silicon (Si) solar cells, which have a diameter of at least 200 µm [1]. In a similar vein, many substitute materials used in thin-film construction can have certain environmental consequences [2].

On the other hand, one of the most promising aspects of photovoltaic devices for converting solar energy into electricity is provided by dye-sensitized solar cells (DSSCs). It functions as a simple, economical, and environmentally beneficial alternative energy conversion technology that is readily scaled up [3]. With a record power conversion efficiency (PCE) of less than 14%, DSSCs have become more and more popular as an efficient and cost-effective replacement for solar devices, according to recent studies [4], [5]. The cost-effectiveness, ease of use, and attractiveness to the environment are only a few of the DSSC's many noteworthy qualities [6]. Additionally, the method used for the dyes' extraction and purification directly affects how well the devices work. Comparing the extracts to the crude, a strong absorption and purification of the extracts was seen. This is explained by the extracts' suppression of absorption [7]. The purification process aims to improve the photophysical and electrochemical properties required for the solar in the following way:

i. the dye must be luminescent.
ii. the dye should cover wide electromagnetic spectra ranging from ultraviolet to infrared regions.
iii. co-absorbents should be added to prevent formation of aggregates and minimize recombination effects.

The frequently used photoanode in DSSC fabrication is TiO_2 due to its unique qualities, which include ease of use, affordability, and biocompatibility. The dye molecules readily

* **CORRESPONDING AUTHOR** | R. A. Akwolu, ✉ rita.akwolu@unn.edu.ng

attach themselves to the TiO_2 nanocrystalline surface because of the structure's porosity and the electrode's large surface area, which inevitably raises the absorption at the semiconductor surface [8]. A bonding is formed between the connecting materials as a result of dyes adhering to TiO_2. To balance the charge transfer and generate the so-called type-II hetero-structure, the donor material gains more holes as a result of the pristine material receiving an additional electron [9]. As a result, as dyes build up on the precursor, electrons are stimulated to transfer to TiO_2, forming a hole in the process that lowers the bandgap energy of the dye/TiO_2 mixture.

On the other hand, compared to standard sorption-ion exchange, photo-catalytic methods for heavy metal exclusion have this property [10]. The performance of the standard type-II hetero-junction is affected by the recombination processes of the hole-electron pair. The hole-electron pairs produced by photo-excitation on the TiO_2 surface cannot be freed by the connection. However, because of the internal electric field and the band alignment effect, the p-n hetero-junction as reported by [11] is more efficient than the conventional type-II hetero-junction.

The reported constraints may also explain why the primary PCE to Si in thin-film solar cell devices is somewhat lower. By creating p-n hetero-junctions, an electric field can be created inside the systems to lessen these difficulties and increase the hole-electron separation in TiO_2. For instance, combining n-type TiO_2 with another p-type semiconductor, such as Cu_2O, to form a p-n hetero-junction [12], [13].

1.1 DSSCs Mechanism of Operation

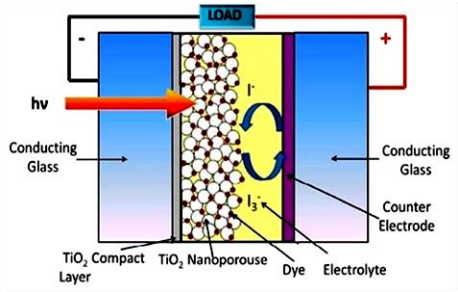

Figure 1: Image showing the mechanism operation of DSSCs [14].

As seen in Figure 1, the fundamental principles of DSSCs operation revolve around optical absorption, carrier transport, electron injection, and current collection. By absorbing light that strikes the surface, the dye, or photosensitizer, excites electrons from their ground state and causes the dye to absorb. A small amount of photons from the ultraviolet area can be absorbed by titanium dioxide thanks to the conduction band's absorption of the photoanode's excited electrons [15]. The dye oxidizes as a result of this absorption of photons. The injected electrons travel between the nanoparticles of titanium dioxide and arrive at the back-contact. The produced electrons promote dye renewal by traveling to the counter electrode via the external circuit.

After being reduced to an ionic state, the oxidized material diffuses to the counter electrode. When sunlight strikes the semiconducting layers, only a small portion of the light is absorbed in the UV range. After that, the working electrode is submerged in a solution that includes the sensitizer and a solvent. When the film is immersed in a dye solution, covalent connections are created between the photoanode's surface and the prepared dye. When the electrode is highly porous and has a large surface area, more dye molecules adhere to the TiO_2 surface.

1.2 Limitations of DSSCs

The limitations encountered by DSSCs[8] include:

i. extrinsic instability from the seal due to a build- up of pressure within the cell.
ii. intrinsic instability.
iii. energy loss of oxidized dye during the regeneration process.
iv. no energy alignment between the electrolyte and oxidized dye.
v. difficulty in scaling dye sensitized devices.
vi. chemical aggressiveness of the electrolyte.
vii. the small modules used increase leaks and reduced cell activity

To raise the effectiveness and performance of DSSCs: Sealants (made from glass frits of low melting point) can be used to minimize leaks from the electrolyte. Others include:

i. transparent conducting oxide can be made more conductive and less resistive by combining indium-doped tin oxide (ITO) and fluorine-doped tin oxide (FTO). ITO has high conductivity with low chemical stability, while FTO has less conductivity with more chemical stability.
ii. glasses can be pretreated with metallic oxide particles to improve their adhesiveness.
iii. subjecting DSSC to a temperature of 80 °C is a good way of improving the cell's intrinsic stability.
iv. the oxidized dye should be reduced rigidly to its initial ground state after the electron is injected. This can be achieved by making the regeneration process faster than the dye oxidation.
v. the rate of dye absorption can be increased by increasing the porous nature of the titanium dioxide nanoparticles.
vi. dark current formation can be limited by depositing the photoanode on the conducting glass.
vii. the working electrode should be uniformly sensitizer by a sensitizer.
viii. relatively inexpensive, light-weight, and easily synthesized materials can be used to enhance the performance of DSSCs.
ix. the photoanode can also be pre-treated with titanium dichloride, $TiCl_4$.
x. interface between the dye and TiO_2 can improve the performance of the cell by lowering the vapor pressure of the solvent.

2 Materials and Methods

2.1 Materials

Vegetable dye extracts from plants found in Nigeria, one of the sub-Saharan African countries, were sampled for the study. They were gathered to create photosensitizers for DSSCs, and they include *Lawsoniainermis* (Laali), *Baphianitida* (Uhie), *Beta vulgaris* (Beetroot) and *Indigoferatinctoria* (Indigo green and red). Without further purification, reagents like calcium hydroxide, ethanol, acetic acid, distilled water, and colloidal titanium dioxide powder (purity 99.9%) were utilized.

2.2 Extraction of Dyes

The plants in the Igboeze North Local Government Area of Enugu state provided samples of *Lawsoniainermis* (Laali), *Baphianitida* (Uhie), and *Beta vulgaris* (Beetroot). The dyes were extracted from the samples using organic solvents like distilled water, ethanol, and acetic acid at room temperature. Lastly, 20 grams of indigo extract, 5 grams of calcium hydroxide, 5 grams of fructose powder, and 5 grams of organic henna powder were mixed to prepare natural indigo for *Indigoferatinctoria* dye.

2.3 Purification of Dyes

Dichloromethane (DCM), an organic solvent, and column chromatography are used in the purification process to separate impurities and other solutions and to obtain the pigment that is responsible for each dye. The purification aids in the impurity removal process.

2.4 Deposition Techniques

In this work, the TiO_2 photo-anodes were deposited using the Doctor Blade methods. The low temperature and cheap processing cost of this technology led to its adoption. Using the commercially available TiO_2 (Anatase), TiO_2 paste was made. To prepare the TiO_2 paste, 2g of TiO_2 powder (P25 Degussa), 5 ml of acetic acid, and 2 drops of Triton-X 100 were mixed in a mortar and milled for 30 minutes. The milling process provided the required high shear pressures, lump-free surface preparation. To get a homogeneous coating, a clean stirring glass rod was utilized to distribute the film. To get rid of any loose particles, ethanol and acetone were used to rinse the samples after deposition. For the films to have a suitable thickness and stability, they were calcined at 450 ℃ and then allowed to cool to room temperature.

2.5 Characterization Techniques

Using an X-ray powder diffractometer, the depositions were analyzed in order to examine the crystallite size, micro strain, and dislocation densities. By utilizing a concentrated electron beam to scan a material's surface at 20 µm and 20.0 kV, scanning electron microscopy (SEM) creates images of the material and analyzes its morphology. Analysis using energy-dispersive spectroscopy (EDS) provided more details about the elemental compositions. To estimate the charge carrier characteristics, Electrochemical Impedance Spectroscopy (EIS) was used. In order to evaluate the photoelectric conversion efficiency and the fill-factor (FF) of DSSCs, I–V characterizations of the fabricated cells were used to estimate the photoelectrical parameters of DSSCs using a simulated sunlight source (A.M 1.5).

3 Results and Discussions

3.1 XRD Analysis

The XRD data studied is shown in Figure 2. The Scherer Equations 1 – 5 were used to obtain the samples' crystallite size (D_p) and interplanar distance (d), lattice parameter, dislocation density, and micro strain, respectively:

$$D_p = \frac{k\lambda}{\beta cos\theta}, \quad (1)$$

$$d = \frac{n\lambda}{2sin\theta}, \quad (2)$$

$$\frac{1}{d^2} = \frac{h^2 + k^2}{a^2} + \frac{l^2}{c^2}, \quad (3)$$

$$\delta = \frac{1}{D_p^2}, \quad (4)$$

$$\varepsilon = \frac{\beta}{4tan\theta}, \quad (5)$$

where k, β, θ = shape factor, full width at half maximum (FWHM), and Bragg's angle respectively. The values of K are commonly accepted as k = 0.94 was used in this work [15] – [16].

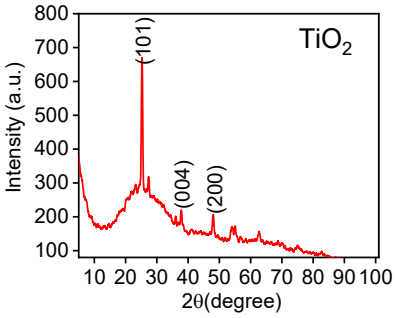

Figure 2: XRD of TiO_2 obtained using a thermally treated doctor blade deposition technique. JCPDS no. 00-064-0863

Table 1: The estimated parameters from XRD

Sample	2θ	FWHM	$D_{p,av}$ (nm)	δ_{av} $\times 10^{-3}$ (nm^{-2})	ε $\times 10^{-3}$	d (Å)
TiO_2	25.23	0.6140	16	3.91	7.10	3.5261

The computed mean crystallite size indicates that this methodology provides a feasible approach to the film preparation required for device manufacturing. The samples' crystalline structure demonstrates the TiO_2 deposition.

Table 1 displays the value results of the computations. The values found can be attributed to the influence of interatomic diffusion on the atoms [16] and the possible existence of additional phases, such as rutile [17]. Larger strain levels

observed, however, may cause cracks or interfere with the films' ability to attach, which could negatively impact the device's functionality.

3.2 Morphological studies

A focused electron beam is utilized in SEM photography at 20 µm and 20.0 kV to create photographs of a material [18]. It displays particle aggregation, which we attributed to the van der Waals force and which is frequently seen during the nanoparticle production process [19].

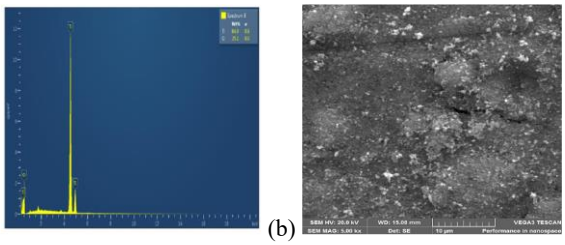

(a) (b)

Figure 3: a.) EDS spectra, b.) SEM micrograph of the deposited TiO_2 films

The TiO_2 NPs film picture shown in Figure 3 was irregularly sphere-shaped and spongy in appearance. It is stated that this morphology is essential for the production of high-performing DSSCs [20]. Furthermore, it is claimed that the spongy characteristic enables maximum dye adsorption and excellent dye absorption into the TiO_2 matrix, both of which would result in effective light harvesting. However, the films also appeared to have a break in the SEM picture (Fig. 3b), which could be the result of greater strain values as shown by the XRD analysis. As no other element was observed, the EDS spectra (Fig. 3a) revealed the elemental composition of Ti and O with weight rates of 64.9 and 35.1 of the film; this is within the range of the manufactured precursor [20], [21].

3.3 UV-Vis Characterizations

The relation in Equation 6 was used to estimate the energy bandgap (E_g) for the samples [15]:

$$(\alpha h\nu)^{1/n} = \beta(h\nu - E_g) \quad (6)$$

Indirect energy band gap obtained through extrapolation of Tauc's plot, $(\alpha h\nu)^{1/n}$ against the photon energy ($h\nu$) to the x-axis yields the material's bandgap.

Table 2: Evaluation of the band gap values for the non-purified samples

Photosensitizers	Distilled water (eV)	Ethanol (eV)
Beta vulgaris (Beet root)	0.94	0.96
Lawsoniainermis (Laali)	0.81	0.78
Indigoferatinctoria (RG)	0.95	0.98
Indigoferatinctoria (GG)	0.88	0.87
Baphianitida (Uhie)	0.90	0.90

The bandgaps as shown in Table 2 illustrate how the samples' vary. For dye extractions, polar solvents work better, such as ethanol, methanol, and distilled water [22]. Among the solvents used for dye extraction, ethanol is said to perform better in photovoltaic applications [23]. As illustrated in Figure 5, the bandgap grows as the absorption peak increases. The samples' purification is credited with the increment [24].

In Figure 6, the charge transfer resistance is estimated by the parallel resistor-capacitor (RC) circuit's impedance response [16], [17]. The diameters of the non-purified photosensitizer were 51.47 Ω, 39.63 Ω, 28.06 Ω, and 44.72 Ω. Within the electrolyte interface and the counter electrodes, charge transfer resistance happened at the high frequency of the semicircle.

On the other hand, the diameters of the purified photosensitizer were 31.47 Ω, 20.96 Ω, 14.04 Ω, and 44.20 Ω. An appropriate equivalent-circuit model is used to fit the AC signal's response in order to obtain the relevant parameters of electron transfer reactions. An example of a circuit that calculates the charge transfer resistance is a parallel resistor-capacitor (RC) circuit. At the interface between the electrolyte, dye, and TiO_2 electrodes in the mid-frequency range, electron transfer resistance happened.

Moreover, the recombination rate and current loss increase with radius [18]. In contrast, impurities in the non-purified dyes caused them to exhibit greater resistance, which could lead to the device's internal shunting elements becoming less effective. The reaction at intermediate frequencies is related to a high capacitance that is a result of electron and redox species accumulation under open-circuit circumstances at the TiO_2 electrolyte interface. Because the I^{3-}/I^- species in the electrolyte have more downward mobility, the response at low frequencies is related to diffusion processes in the electrolyte. These were discovered to be compatible with [17].

3.4 I–V Characteristics of the DSSCs

Using a simulated sunshine source (A.M 1.5), the power conversion efficiencies (PCE) of DSSCs were computed. These speak of the use of an artificial light source that, at the same intensity as the typical solar spectrum at ground level, replicates the spectrum of solar radiation. The average path length of solar radiation through the earth's atmosphere at a zenith angle of 48.2 degrees is known as air mass 1.5 or A.M. 1.5.

The ability of the device to convert incident light into electricity is measured in order to determine the photoelectric conversion efficiency of DSSCs. Since the A.M. 1.5 spectrum is relevant to real-world solar conditions, it is important to use a light source that closely replicates the spectrum of light.

The values of maximum current (I_{max}), maximum voltage (V_{max}), open-circuit voltage (V_{oc}) and short-circuit current (I_{sc}) were deduced from the I–V characteristic plots as shown in Figure 7 for the purified Dye samples. The estimated fill-factor (FF) and efficiency (η %) were calculated using 1000 W/m^2 for the incident photons over 3.5 cm^2.

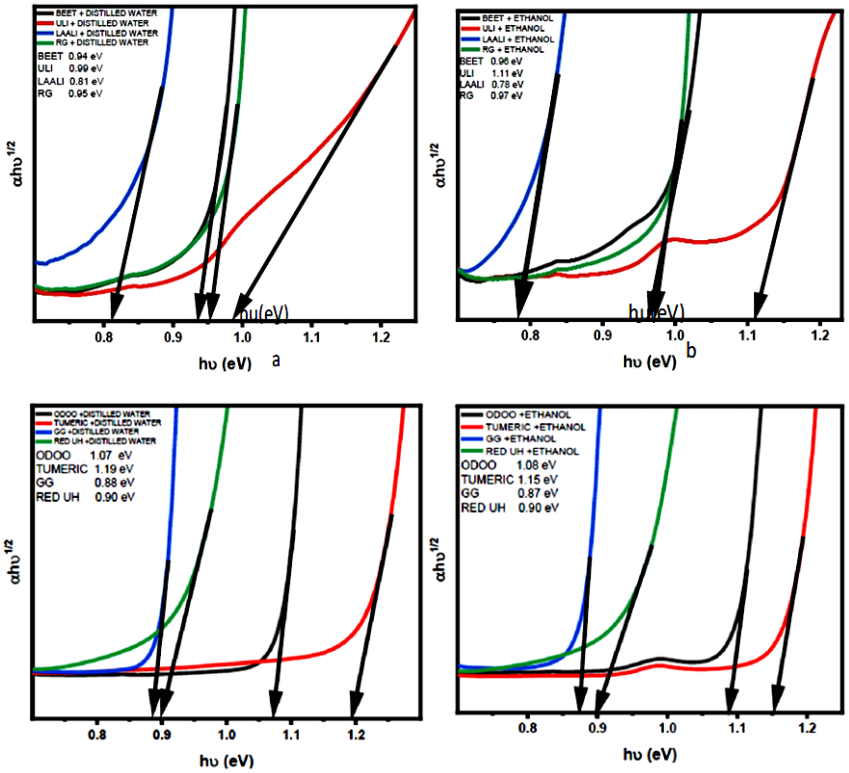

Figure 4: Energy bandgap for the samples.

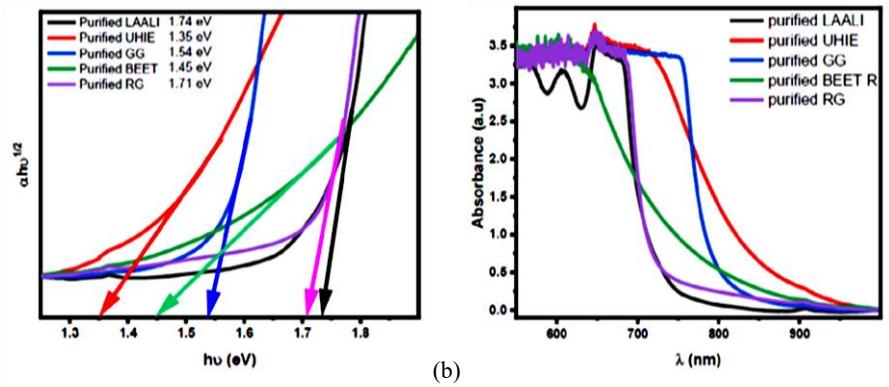

Figure 5: a.) Energy bandgap and b.) the measured absorbance spectra.

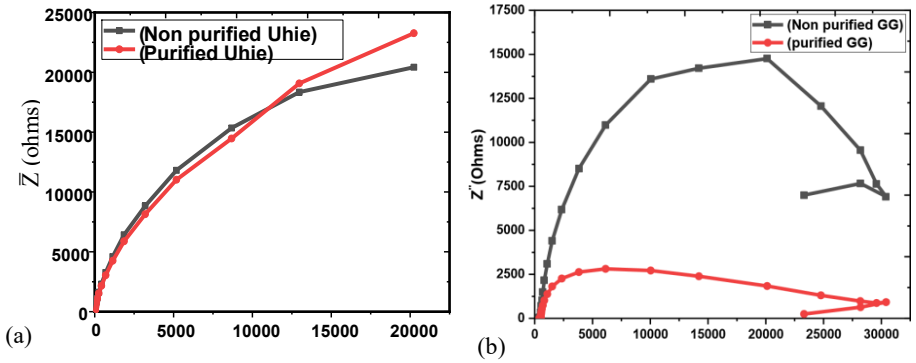

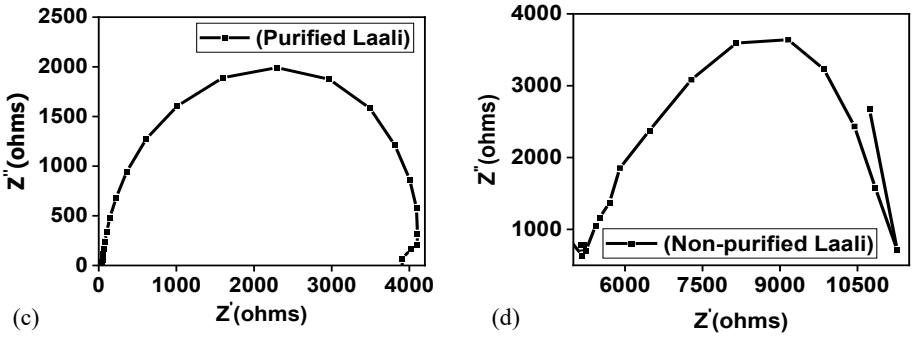

Figure 6: Nyquist plots of EIS spectra of the fabricated DSSCs for non-purified, purified and combined purified dyes.

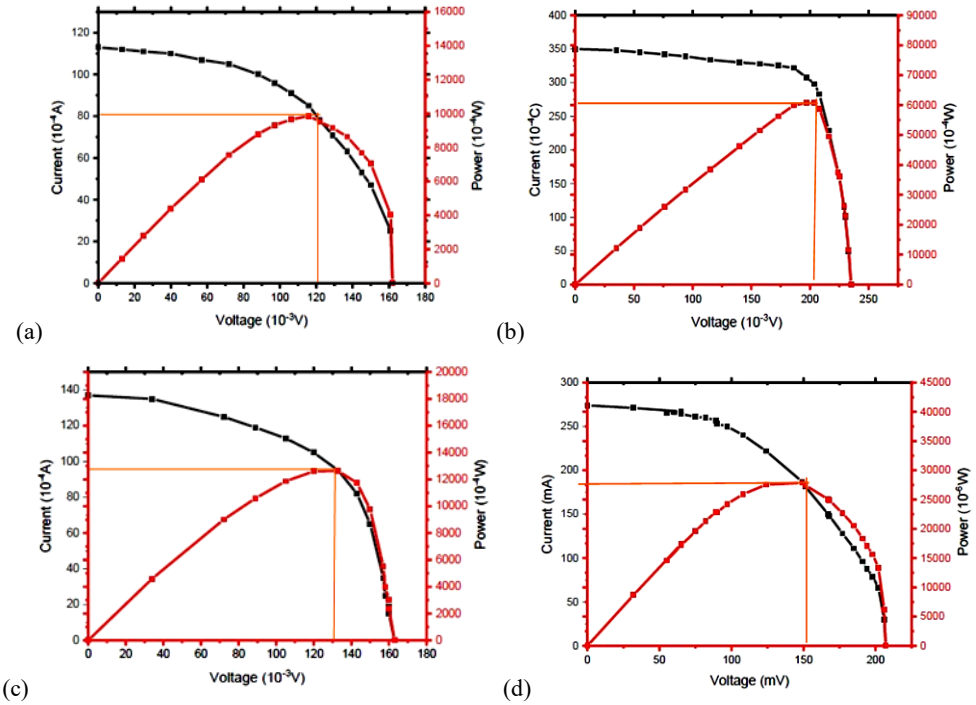

Figure 7: The I–V curves for the DSSCs fabricated from purified dyes of a.) Green Indigoferatinctoria (GG) b.) Lawsoniainermis (Laali) c.) red Indigoferatinctoria (RG) and d.) Baphianitida (Uhie).

Table 3: Summary for the DSSCs from the non-purified dyes.

Sample	I_{sc} (mA)	V_{oc} (mV)	I_{max} (mA)	V_{max} (mV)	FF	PCE (%)	R_{ct} (ohms)
Laali	22.0	219	18.4	163	0.66	0.32	51.47
Uhie	28.3	157	194	165	0.69	0.48	28.07
GG	11.3	157	5.39	116	0.30	0.13	39.63
RG	13.7	129	6.40	149	0.22	0.10	44.72

Table 4: A summary of photovoltaic parameters for the DSSCs fabricated using the purified photosensitizers

Sample	I_{sc} (mA)	V_{oc} (mV)	I_{max} (mA)	V_{max} (mV)	FF	PCE (%)	R_{ct} (ohms)
Laali	35.0	235	29.8	204	0.74	1.74	14.04
Uhie	27.4	149	187	150	0.61	1.11	20.96
GG	11.3	162	8.50	116	0.54	0.28	31.47
RG	13.7	133	9.50	163	0.85	0.44	44.20

The estimated values for the different dye performances, as in Table 3, show results that have some improvements and comparable efficiencies for DSSCs.

Conversion efficiencies of 0.32%, 0.48%, 0.13%, and 0.10% were produced by DSSCs fabricated with non-purified Laali, Uhie, GG, and RG, respectively. When comparing the photovoltaic performance of devices made with Uhie dye to those made with other dyes, the former's RG showed lower values in contrast to those in Table 4, fabricated using purified photosensitizers.

Computed results for non-purified dyes show greater resistance at the interface between the semiconductor oxide and electrolyte, supporting the results of charge transfer resistance. This adversely influences the charge transfer and makes the cell less functional. These results have implications for charge

transfer resistance; a higher charge transfer resistance could result in a worse overall efficiency for the DSSC.

When they encounter considerable resistance, the photo-generated electron-hole pairs may recombine rather than aggregate, which would reduce the cell's overall energy conversion efficiency and current output. It can also lower the open circuit voltage of the DSSC due to the higher voltage loss caused by internal resistance. By preventing charges from passing through, a greater R_{ct} can reduce short circuit current and consequently the photocurrent that the cell generates. The poor performance is caused by a variety of variables and directly reduces the efficiency of solar cells. Among these is the structure of the pigment, which prevents molecules from efficiently arraying on the TiO_2 film and acts as a steric impediment to the pigment's capacity to form a connection with the TiO_2 oxide surface [25].

This means that electrons from the dye molecules will not move to the conduction band of the TiO_2 film. The range and intensity of light absorption of natural pigments, the distance between the location on the TiO_2 surface and the dye skeleton that facilitates electrons moving from the dye molecule to the surface, and the pigments' aggregation and masking effects, which decrease their interaction with the TiO_2 surface and the absorption of visible light, respectively [26].

4 Conclusions

This study focused on using dichloromethane and column chromatography, two polar solvents, to extract and purify natural dyes. Using a doctor blade technique, we deposited TiO_2 films on an FTO glass substrate, and we then calcined the film at 450 °C. On TiO_2 thin films, the drop casting deposition of dyes technique was also applied. Natural dyes were used to gather photosensitizers. In light of this research, we showed that anatase structural phases were successfully deposited, according to the XRD diffractograms. Agglomerated sample morphology was noted. The charge transfer process between the dyes and TiO_2 was also shown to have potential explanations by the EIS analysis. The photoelectrical characteristics of DSSCs were estimated by the I–V characterizations. To sum up, this study's findings show that purified dye samples significantly enhance the PCE of dye photosensitizers.

Acknowledgment

Rita A. Akwolu would like to express her heartfelt gratitude to the brilliant researchers at the Department of Physics and Astronomy, University of Nigeria, Nsukka, for their invaluable support throughout this project. Special thanks are extended Prof. F. Ezema, Ass. Prof. Mrs. A.N.C. Agbogu for their unwavering guidance, insightful advice, and encouragement. Their constant support, both academic and personal, has been a significant source of inspiration and motivation for the successful completion of this work. Additionally, Rita is deeply grateful for the prayers and well-wishes from all those involved, which helped to sustain her throughout this research.

Authors' Credit Statement

R. A. Akwolu, K. P. Alor, C.O. Ayogu, conceptualization, methodology, data analysis, graphical plots, writing of original draft; **R. A. Akwolu, P.U. Asogwa,** editing, proofreading and manuscript handling; **R. A. Akwolu, K. P. Alor,** supervision and suggestions.

Declaration of Competing Interest

The authors declare no personal or financial conflicts that may influence the research presented in this paper.

References

[1] E. Klugmann-Radziemska, P. Ostrowski, K. Drabczyk, P. Panek, and M. Szkodo, "Experimental validation of crystalline silicon solar cells recycling by thermal and chemical methods," *Sol. Energy Mater. Sol. Cells*, vol. 94, no. 12, pp. 2275–2282, 2010, doi: 10.1016/j.solmat.2010.07.025.

[2] P. Sinha, "Potential environmental hazards of photovoltaic panel disposal: Discussion of Tammaro et al. (2015)," *J. Hazard. Mater.*, vol. 323, pp. 733–734, 2017, doi: 10.1016/j.jhazmat.2016.04.021.

[3] R. L. Vekariya, K. K. Sonigara, K. B. Fadadu, J. V. Vaghasiya, and S. S. Soni, "Humic Acid as a Sensitizer in Highly Stable Dye Solar Cells: Energy from an Abundant Natural Polymer Soil Component," *ACS Omega*, vol. 1, no. 1, pp. 14–18, 2016, doi: 10.1021/acsomega.6b00010.

[4] M. Green, E. Dunlop, J. Hohl-Ebinger, M. Yoshita, N. Kopidakis, and X. Hao, "Solar cell efficiency tables (version 57)," *Prog. Photovoltaics Res. Appl.*, vol. 29, no. 1, pp. 3–15, 2021, doi: 10.1002/pip.3371.

[5] C. P. Lee, C. T. Li, and K. C. Ho, "Use of organic materials in dye-sensitized solar cells," *Mater. Today*, vol. 20, no. 5, pp. 267–283, 2017, doi: 10.1016/j.mattod.2017.01.012.

[6] Q. Dai and J. Rabani, "Unusually efficient photosensitization of nanocrystalline TiO2 films by pomegranate pigments in aqueous medium," *New J. Chem.*, vol. 26, no. 4, pp. 421–426, 2002, doi: 10.1039/b108390b.

[7] H. K. Lee, "Talk Louder So I Can See You," *Neuron*, vol. 89, no. 5, pp. 887–888, 2016, doi: 10.1016/j.neuron.2016.02.026.

[8] K. Sharma, V. Sharma, and S. S. Sharma, "Dye-Sensitized Solar Cells: Fundamentals and Current Status," *Nanoscale Res. Lett.*, vol. 13, 2018, doi: 10.1186/s11671-018-2760-6.

[9] J. Low, B. Cheng, and J. Yu, "Surface modification and enhanced photocatalytic CO 2 reduction performance of TiO 2 : a review," *Appl. Surf. Sci.*, vol. 392, pp. 658–686, 2017, doi: 10.1016/j.apsusc.2016.09.093.

[10] M. Babudurai *et al.*, "Mechanical activation of TiO2/Fe2O3 nanocomposite for arsenic adsorption: effect of ball-to-powder ratio and milling time," *J. Nanostructure Chem.*, vol. 11, no. 4, pp. 619–632, 2021, doi: 10.1007/s40097-021-00388-8.

[11] M. Irimia-Vladu, "'Green' electronics: Biodegradable and biocompatible materials and devices for sustainable future," *Chem. Soc. Rev.*, vol. 43, no. 2, pp. 588–610, 2014, doi: 10.1039/c3cs60235d.

[12] B. Sun, G. Zhou, T. Gao, H. Zhang, and H. Yu, "NiO nanosheet/TiO 2 nanorod-constructed p-n heterostructures for improved photocatalytic activity," *Appl. Surf. Sci.*, vol. 364, pp. 322–331, 2016, doi: 10.1016/j.apsusc.2015.12.158.

[13] Y. Zhao *et al.*, "Fabrication of BiOBr nanosheets@TiO 2 nanobelts p-n junction photocatalysts for enhanced visible-light activity," *Appl. Surf. Sci.*, vol. 365, pp. 209–217, 2016, doi: 10.1016/j.apsusc.2015.12.249.

[14] Baig, M. M. (2021). Solar cells and its applications. *International Journal of All Research Education and Scientific Methods*, *7*, 3493-3500

[15] H. Kusama, H. Orita, and H. Sugihara, "TiO2 band shift by nitrogen-containing heterocycles in dye-sensitized solar cells: A periodic density functional theory study," *Langmuir*, vol. 24, no. 8, pp. 4411–4419, 2008, doi: 10.1021/la703696f.

[16] E. O. Onah *et al.*, "Comparative photo-response performances of dye sensitized solar cells using dyes from selected plants," *Surfaces and Interfaces*, vol. 20, no. August, 2020, doi: 10.1016/j.surfin.2020.100619.

[17] A. F. Nogueira, C. Longo, and M. A. De Paoli, "Polymers in dye sensitized solar cells: Overview and perspectives," *Coord. Chem. Rev.*, vol. 248, no. 13–14, pp. 1455–1468, 2004, doi: 10.1016/j.ccr.2004.05.018.

[18] Z. He, J. Li, D. Wang, J. Wang, and T. Zhang, "Enhanced photovoltaic performance of TiO2 dye-sensitized solar cell based on one-dimensional composite photoanode," *Int. J. Electrochem. Sci.*, vol. 12, no. 10, pp. 8918–8928, 2017, doi: 10.20964/2017.10.02.

[19] X. Deng, Z. Huang, W. Wang, and R. N. Davé, "Investigation of nanoparticle agglomerates properties using Monte Carlo simulations," *Adv. Powder Technol.*, vol. 27, no. 5, pp. 1971–1979, 2016, doi: 10.1016/j.apt.2016.06.029.

[20] A. Machrouhi *et al.*, "Effectiveness of beetroot seeds and H3PO4 activated beetroot seeds for the removal of dyes from aqueous solutions," *J. Water Reuse Desalin.*, vol. 8, no. 4, pp. 522–531, 2018, doi: 10.2166/wrd.2017.034.

[21] W. Li and T. Zeng, "Preparation of TiO2 anatase nanocrystals by TiCl4 hydrolysis with additive H2SO4," *PLoS One*, vol. 6, no. 6, pp. 2–7, 2011, doi: 10.1371/journal.pone.0021082.

[22] O. Adedokun, Y. K. Sanusi, and A. O. Awodugba, "Solvent dependent natural dye extraction and its sensitization effect for dye sensitized solar cells," *Optik (Stuttg).*, vol. 174, pp. 497–507, 2018, doi: 10.1016/j.ijleo.2018.06.064.

[23] M. K. Hossain *et al.*, "Effect of dye extracting solvents and sensitization time on photovoltaic performance of natural dye sensitized solar cells," *Results Phys.*, vol. 7, pp. 1516–1523, 2017, doi: 10.1016/j.rinp.2017.04.011.

[24] Z. Xu, Y. Li, and Z. Liu, "Boron, nitrogen, and nickel impurities in GeC nanoribbons: A first-principles investigation," *J. Magn. Magn. Mater.*, vol. 433, pp. 53–58, 2017, doi: 10.1016/j.jmmm.2017.02.054.

[25] H. Zhou, L. Wu, Y. Gao, and T. Ma, "Journal of Photochemistry and Photobiology A : Chemistry Dye-sensitized solar cells using 20 natural dyes as sensitizers," *"Journal Photochem. Photobiol. A Chem.*, vol. 219, no. 2–3, pp. 188–194, 2011, doi: 10.1016/j.jphotochem.2011.02.008.

[26] M. R. Narayan, "Review: Dye sensitized solar cells based on natural photosensitizers," *Renew. Sustain. Energy Rev.*, vol. 16, no. 1, pp. 208–215, 2012, doi: 10.1016/j.rser.2011.07.148.